arXiv:1011.3103v2 [astro-ph.HE] 2 Dec 2010

Multiband Fitting to Three Long GRBs with Fermi/LAT Data: Structured Ejecta Sweeping up a Density-Jump Medium

S. Y. Feng[1,2], Z. G. Dai[1,2]

[1]*Department of Astronomy, Nanjing University, Nanjing 210093, China;*
[2]*Key Laboratory of Modern Astronomy and Astrophysics (Nanjing University), Ministry of Education, Nanjing 210093, China;*
siyifeng@msn.com. dzg@nju.edu.cn

ABSTRACT

We present broadband (radio, optical, X-ray and GeV) fits to the afterglow light curves and spectra of three long-duration gamma-ray bursts (GRBs 080916C, 090902B, and 090926A) detected by the Gamma-Ray Burst Monitor (GBM) and Large Area Telescope (LAT) instruments on the Fermi satellite. Using the observed broadband data, we study the origin of the high energy emission, and suggest that the early-time GeV emission and the late-time radio, optical, and X-ray afterglows can be understood as being due to synchrotron emission from an external forward shock caused by structured ejecta propagating in a wind bubble jumping to a homogeneous density medium. The structured ejecta can well explain the early rising feature of the GeV emission from these bursts and the density-jump medium can account for some certain plateaus or flares in the late afterglows. From our fits, we find that these Fermi-LAT events preferentially occur in a low-density circumburst environment, in which case the Klein-Nishina cutoff effect is significant. Such an environment might result from superbubbles or low-metallicity progenitor stars (which have a low mass-loss rate at late times of stellar evolution) of type Ib/c supernovae.

Subject headings: gamma-rays: bursts — gamma-rays: theory

1. Introduction

Gamma-ray bursts (GRBs) are a kind of astrophysical phenomenon so luminous in the universe that their isotropic energies of $10^{48} - 10^{55}$ergs are usually considered coming from extremely relativistic outflows with bulk Lorentz factors as high as $10^2 - 10^3$. The connection between long-duration GRBs and broad-line SNe Ib/c (low-metallicity) has been supported

by some pieces of observational evidence (Woosley & Bloom 2006). The recently launched Fermi Gamma-Ray Space Telescope with the on-board Gamma-ray Burst Monitor (GBM) and Large Area Telescope (LAT) instruments (Atwood et al. 2009; Meegan et al. 2009) in conjunction with the Swift narrow field instruments (Gehrels et al. 2004) have opened a new era of understanding physical mechanisms of GeV photon emission in very energetic GRBs and their relation to lower-energy afterglow emission. Up to now, several novel yet tricky features have appeared during the whole period of observations and their complexities have challenged the anterior established theoretic models.

The first feature is that the sub-MeV and GeV photons observed by GBM and LAT respectively behave distinctive spectral and temporal properties. The GBM light curves are nearly flat during the main episode of the prompt emission, then drop extremely rapidly (e.g. $t^{-3.3}$ for GRB 080916C (Abdo et al. 2009a)), and eventually cease abruptly. This can also be validated from $\sim 60\%$ of all bursts detected by the Swift satellite (Evans et al. 2009). For the LAT light-curves, however, a rise appearing in the early few seconds ($< T_{90}$) was followed by a single power-law decay without any cutoff up to hundreds of seconds after the GBM trigger, till below the monitor sensitivity, and decay of the late LAT emission was much shallower than the GBM-detected counterparts at the same times (Zhang et al. 2010). Furthermore, the LAT emission usually lags the GBM emission from fractions of seconds to a few seconds. In addition, the spectral slopes of the GBM and LAT emissions are often different, e.g., the GBM data can be fitted with a Band spectrum that is composed of two smoothly-joining power laws, while the LAT data are often fitted by a power law with a slope intermediate between the two slopes of the GBM fit. These properties seem to indicate that the high-energy emission and low-energy emission detected by LAT and GBM have different origins.

The temporal properties of the LAT emission have been studied, and some explanations differing in the source's dominant component have been proposed. A prevalent explanation is particle-dominated models. One inclination is the leptonic interpretation. Because of their distinctive light curve properties we mentioned above, it is highly probable that the MeV photons may be of an internal origin, while the GeV photons may be generated via synchrotron emission of electrons accelerated by an external forward shock that also leads to lower-energy afterglow emission (Kumar & Barniol Duran 2009). Wang et al. (2009, 2010) studied the Klein-Nishina effect on the high-energy afterglow emission and found that at early times such an effect strongly suppressed the inverse Compton scattering of those electrons that produced the high-energy emission. Thus synchrotron radiation of the electrons becomes a plausible mechanism. This conclusion was independently drawn by Zhang & Pe'er (2009), who suggested that the lack of a thermal component in the GBM spectrum of GRB 080916C is consistent with a relativistic Poynting-flux-dominated outflow.

The explanation of synchrotron radiation of the electrons accelerated by a forward shock is fairly natural to account for both the observed delay of the > 100 MeV photons and long lasting of their emission. However, thermal component deviating from the smooth Band spectrum function in some bursts (i.e. GRB090510, GRB090902B, GRB090926A) seems to beyond prediction of what is often invoked from the external shock model (Zhang et al. 2010). Moreover, a rapid rise during the first few seconds (e.g. $\sim t^6$ of GRB080916C) is hard to be well explained within such a framework (Toma et al. 2009). Therefore, in addition to the hypothesis of a separate origin, Toma et al. (2009) assumed that GeV and MeV photons may come from the same region, but the onset of the high-energy may result from anisotropic inverse Compton scattering of an optical-thin expanding cocoon, delayed compared with the MeV emission. Nevertheless, in their calculation, this up-scattering cocoon is so short-lived that it could not account for the whole high energy emission.

Another approach is the hadronic scenario. Razzaque et al. (2009) suggested that the MeV and GeV photons could be interpreted as the radiation of accelerated electrons and cosmic ray protons respectively, as well as the delay between them could come from different cooling time scales in a highly magnetized shock. In their framework, the model of GRB 080916C is plausible only when $\Gamma \leq 500$ and the jet opening angle $\sim 1^\circ$. Alternativly, Asano et al. (2009) considered another possibility of the photomeson cascade and proton synchrotron models, and provided their constraint in GRB090510. Notwithstanding, to reproduce the extra component around GeV with these models, the proton injection isotropic-equivalent luminosity is required to be larger than $10^{55}\mathrm{ergs}^{-1}$. Such a large proton luminosity is a challenge for the hadronic models.

All the works mentioned above inspire us to consider a plausible structured outflow, in which the bulk Lorentz factor of the initial shells tends to be lower than that of the late shells and the emitting region may be initially optically thick for GeV photons to escape. This, therefore, would lead to an early rapidly rising light curve and transient soft to hard spectrum.

The second feature of the three long GRBs with LAT data is that some humps or flares appear in the light curves of the $> 10^5$ s low-energy afterglows (Cenko et al. 2010; Swenson et al. 2010). Neglecting this feature, Kumar & Barniol Duran (2010) fitted the multi-band light curves of these GRBs by assuming that a relativistic external shock sweeps up an interstellar medium, and obtained reasonable physical parameters or parameter spaces accordingly. Although their fittings somehow favor the external shock model, humps (or sometimes flares) have indeed been observed on the late-time optical and X-ray afterglow light curves, which do not completely accord with a simple power-law but instead the decay after the humps is shallower than that before the humps. These observations call for a more

meticulous consideration of the external shock model.

It is noted that a density-jump medium proposed by Dai & Lu (2002) has provided us with a clue for some optical and X-ray humps and well fitted to several bursts (Dai & Wu 2003; Tam et al. 2005; Jin et al. 2009). In this scenario, a relativistic jet first expands in a stellar wind, subsequently encounters a density jump, and finally expands in a homogeneous medium. This interaction can produce an observed light-curve bump.

In this paper, we show that the early-time GeV emissions and the late-time radio, optical, and X-ray afterglows of GRBs 080916C, 090902B, and 090926A can be understood as being due to synchrotron emission from an external forward shock caused by structured ejecta propagating in a wind bubble jumping to a homogeneous density medium. In §2 we include a set of observaed broadband (LAT, XRT, UVOT) data on these three luminous long bursts. Then, our model is set up in §3. In particular, The structured ejecta can well explain the universal early rising feature of the GeV emission from these bursts and the density-jump medium can account for some certain plateaus and flares in the late afterglows. Additionally, for the sake of verifying whether or not the lower energy (X-ray, optical, radio) emission originates from the same source as the higher energy (>100 MeV) emission, we discuss the effect of synchrotron self-Compton (synchrotron self-absorption) on the high energy (radio) emission, which, in the constrained parameter space estimated analytically from XRT and UVOT light curves, is proved in §4 having a small contribution to the flux density during the observed period. In this section, we find a reasonable set of parameters which can be valid for most of the late afterglows. Our conclusions concerning a plausible central engine and ambient environment of bright, long GRBs are discussed in §5.

Throughout this work, we adopt the convenience $Q_x = Q/10^x$ in units of cgs.

2. Observations

Among the 19 observed Fermi-LAT GRBs during the first 2 years' operation, GRB080916C, GRB090902B and GRB090926A are 3 typical brightest long GRBs with abundant of spectrum information (Granot 2010).

2.1. GRB080916C

This burst, located at redshift $z = 4.35 \pm 0.15$ (Greiner et al. 2009), is the first GRB detected by Fermi with high significance of photons at energies > 0.1 GeV. The isotropic energy emitted from prompt emission can be estimated as $E_{\gamma,iso} = 8.8 \times 10^{54}$erg (Abdo et al. 2009a).

At 00:12:45.613542 on 16 September 2008 (Abdo et al. 2009a), this GRB was triggered on by GBM with the duration $T_{90} = 66$s. Before $T_0 + 4$s, the LAT light-curve shows an extremely steep rise $F_{\nu,LAT} \propto t^{6\pm0.5}$, followed by a simple power law decay $F_{\nu,LAT} \propto t^{-1.33\pm0.08}\nu^{-1.1\pm0.1}$ until $\sim$ 1400s (Zhang et al. 2010). X-ray and optical photons were detected by XRT and UVOT since 17:11:28 16 September 2008 ($T_0 + 61$ks). A steep decay (to $\sim T_0 + 101$ks) continued with a plateau (to $\sim T_0 + 204$ks) goes to a slightly shallower decay without break until 1.3Ms from the trigger T_0. During the period of $T_0 + 61$ks$-T_0 + 1306$ks, the simple power law light curve and spectrum evolution show the flux density at X-ray band, $F_{\nu,X} \propto t^{-1.29\pm0.09}\nu^{-0.50\pm0.16}$, as well as for the optical band, $F_{\nu,opt} \propto t^{-1.40\pm0.05}\nu^{-0.38\pm0.20}$ (Greiner et al. 2009). Besides, AGILE, RHESSO, INTEGRAL, Konus-Wind, and MESSENGER all provide a plentiful of data information for the late afterglow (Perri et al. 2008).

Many groups have studied this GRB with the external shock model (Kumar & Barniol Duran 2010; Gao et al. 2009; Zou et al. 2009), and suggest the late time afterglow data can be used to extrapolate the early LAT data, as well as be predicted from it, under the preference of circumburst density stratification.

2.2. GRB090902B

This burst is an exceptional case with redshift $z = 1.822$, whose speciality lied in both phases of prompt emission and early afterglow (Abdo et al. 2009b). Unlike majority of the other GRB events, excess emission exhibited in both low ($\leq$ 100keV) and high ($\geq$ 10MeV) band during the prompt emission. Moreover, the soft-hard-soft spectral evolution indicates two components: Band function peaking at $\sim$ 700keV (Table 1) + simple power-law with photon index $\Gamma \sim 1.85$ (Zhang et al. 2010). The isotropic energy release $E_{\gamma,iso} = (3.83 \pm 0.05) \times 10^{54}$erg (Cenko et al. 2010). Explanations of a superpositing quasi-thermal spectrum include the hadronic origin [either proton synchrotron radiation(Razzaque et al. 2009) or photohadronic interactions (Asano et al. 2009)], or thermal emission from the jet photosphere (Ryde et al. 2010).

This burst was triggered and located at 11:05:08.31 on September 2009, by the Fermi-GBM (Bissaldi & Connaughton 2009) and Suzaku-WAM (Terada et al. 2009) with multi-peaked duration $T_{90} \approx 21s$. After a rapid rise until $T_0 + 7$s, the LAT band light-curve decays up to $T_0 + 1$ks with $F_{\nu,LAT} \propto t^{-1.4\pm0.06}$, including an energetic photon detected as high as $11.16^{+1.48}_{-0.58}$ GeV within the prompt emission phase and another $33.4^{+3.7}_{-3.5}$ GeV at $T_0 + 82$s (Abdo et al. 2009b). The Swift XRT (Kennea & Stratta 2009; Evans et al. 2009b; Stratta et al. 2009) and UVOT (Swenson & Siegel 2009) began concurrently target of opportunity of the field of GRB090902B's fading source from 23:36 on 2 September 2009 and

copious of data have been in hand from $T_0 + 0.5$ks. A steep decay (to $\sim T_0 + 116$ks) simultaneously ended with a slight rise in both bands. It is highly possible that jet break occurred at $\sim T_0 + 553$ks (Pandey et al. 2010). During this whole period, the X-ray spectrum evolved as $F_{\nu,X} \propto t^{-1.36\pm0.03}\nu^{-0.90\pm0.13}$, and for the optical band, $F_{\nu,opt} \propto t^{-0.89\pm0.05}\nu^{-0.76\pm0.07}$. In addition, VLA began to observe the afterglow since 3 September 2009 (Chandra & Frail 2009) until 5 months later at 8.5GHz and 4.8GHz.

Kumar & Barniol Duran (2009) have studied this GRB with an external shock model in the monotonic circumburst environment, and concluded that, on one hand, even without making use of the temporal decay indices, the wind medium can be ruled out because an expected late low energy afterglow is brighter than the extrapolation from early high energy data. On the other hand, a uniform density seems to conflict with the observed steep decay, which further disputes a possibility of the same region for prompt sub-MeV and MeV photons. Another discussion comes from Cenko et al. (2010). Using the forward-reverse shock and constant density model, the afterglow of this burst has been better fit in X-ray and radio bands than in the optical/UV band, except for the first point at $\sim 10^4$s. Parameter constraints without taking LAT data into account suggest a low circumburst density and a large kinetic energy, which is possible in the narrow opening angle $\sim 3.4°$. Later, Liu & Wang (2010) have provided a meticulous discussion about the two-component forward-reverse external shock in a monotonic circumburst environment and their calculation was well fit to the four observed bands except for the very early rising part of the LAT light curve.

2.3. GRB090926A

This burst is the GRB detected at $z = 2.1062$ by Fermi with photons as high as ~ 20 GeV at 26s after the trigger (Uehara et al. 2009). The prompt emission time-integrated flux indicates its isotropic emission energy yields $E_{\gamma,iso} = 2.1^{+0.09}_{-0.08} \times 10^{54}$erg (Zhang et al. 2010).

Since the trigger at 04:20:26:26.99 on 26 September 2009, GBM and LAT started operation and found that a single pulse with duration $T_{90} \approx 20s$ can be well modeled by a Band function spectrum (see Table 2) in the prompt emission, along with the Suzaku-WAM (Noda et al. 2009), Konus-Wind (Golenetskii et al. 2009), and RT-2 on CORONAS-PHOTON (Chakrabarti et al. 2009). The light curve rose slightly for quite a few seconds (to $\sim T_0 + 16$s), and decayed $F_{\nu,LAT} \propto t^{2.05\pm0.14}\nu^{-1.26^{+0.24}_{-0.22}}$. A fading X-ray counterpart was observed by XRT since 17:17 on 26 September ($T_0 + 46.7$ks) (Vetere et al. 2009), then PROMPT, SMARTS detected photons in several optical filters but no radio (5.5GHz) source under the limit of 1.5mJy was detected up to 1 October 2009. As shown on the light curve, a

plateau ($T_0+51.4$ks $\sim T_0+92$ks) overlaps the simple power law decay that is slightly steeper than the fading supposed to be extrapolated from the early trace. No break up to 100ks from the trigger T_0 was observed. During the period from $T_0 + 46.7$ks to $T_0 + 149$ks, two variabilities, are suggested to be flares (the first, at ~ 70ks $- 95$ks with $\delta t/t \approx 0.35$; the second is slight, at 195ks-260ks, with $\delta t/t \approx 0.28$) overly on the simple power law light curve in both X-ray band ($F_{\nu,X} \propto t^{-1.40\pm0.05}\nu^{-1.6^{+0.3}_{-0.2}}$) and optical band ($F_{\nu,opt} \propto t^{-1.01^{+0.03}_{-0.07}}\nu^{-1.77^{+0.26}_{-0.21}}$) (Swenson et al. 2010).

Cenko et al. (2010) and Rau et al. (2010) studied the later afterglow (X-ray, optical) of this burst, provided certain parameter space, confirmed the second flare, and indicated that the jet break occurs around ~ 21d. However, due to lack of radio data, the constraints cannot be narrowed down. Meanwhile, as for a common rebrightening plateau in 5 optical bands, they suggested a density-jump circumstance (e.g., Dai & Lu 2002; Lazzati et al. 2002; Tam et al. 2005) or a smooth injection of energy into the forward shock from the central engine (e.g.,Dai & Lu 1998a; Rees & Meszaros 1998), and called for a detailed analysis for the early higher energy emission.

3. Model

The behavior of the GRB afterglows shed light on the external shock model (Panaitescu & Kumar 2002). A collimated ($\theta \leq 10°$), ultrarelativistic outflow of matter and/or radiation is driven by a central engine. Certain dissipative processes within the outflow give rise to the prompt gamma-ray emission, with a fraction $\varsigma_\gamma \equiv E_{\gamma,iso}/(E_{\gamma,iso} + E_{K,iso})$ of the total relativistic energy converted to high-energy radiation.

A self-consistent result of the multiband (X-ray, optical, radio) afterglow data coordinated with the prompt emission relics producing > 100MeV photons, may support the external shock origin of LAT photons, which is the same as the later lower-band emission. Although the LAT-band activities seem to track the GBM-band activities and indicates an internal shock origin of the high energy photons (Zhang et al. 2010), the decay of these two components are inconsistent. Therefore, in this piece, we take no consideration of the GBM emission. Moreover, the particularities of GRB 090902B we mentioned above may evoke doubts about the conventional external shock + monotonic circumstance model (we will discuss it in §5), but it enlightens our deliberate consideration on amendment to structured ejecta sweeping up the density-jump medium.

3.1. Dynamics

3.1.1. Before the Deceleration Time

Materials can be ejected by a central engine continuously during a period $\triangle t$ (which is in the T_{90} region of prompt emission). We here suggest, within the framework of the collapsar model, an increase of the Lorentz factor of the ejecta in active times of the central engine for two reasons. First, angular momentum of the accreted fall-back matter would spin up the central compact object and thus its rotational energy loss could give rise to an increase of the ejecting luminosity. Second, earlier-ejected shells, when breaking through the stellar envelope, may suffer from more massive baryon contamination, and thus later-ejected shells may propagate in a tunnel (the later the cleaner). Therefore, the Lorentz factor of the ejecta head may increase with time. For simplicity, we assume the bulk Lorentz factor of the front materials distribute as a power-law function of time: $\Gamma \propto t^s$ for $t \leq \triangle t$.

We denote $M_{\rm ej}$ as the accumulated mass ejected by the central engine at some certain time, and η as the bulk Lorentz factor of a blast wave at this certain time, which is defined when the mass of the surrounding matter swept up by the blast wave, $M_{\rm sw}$, is equal to $M_{\rm ej}/\eta$. After this time, the bulk Lorentz factor presents an obvious deceleration, contributing to a peak of the LAT light curve. This time is called the deceleration time, and we believe that it meets with other physical turning points, e.g., the central engine stops patently ejecting or photosphere becomes transparent almost in the meanwhile.

The shock propagates a distance $\delta R \sim 2\Gamma^2 c\delta t/(1+z)$ during a small observed time δt. Integrating this using the scaling law, one obtains $t = (1+z)R/[2(4-k)\Gamma^2 c]$. Therefore, in a homogeneous ($k=0$) or wind ($k=2$) medium with circumburst density $n = AR^{-\rm k} = 10^{35.5}A_{35.5}R^{-\rm k}$ (Sari et al. 1998; Dai & Lu 1998b; Chevalier & Li 2000), when

$$t_{\rm dec} = \frac{(1+z)R_{\rm dec}}{2(4-k)\eta^2 c} = \begin{cases} 2.6\,{\rm s}E_{\rm K,53}^{1/3}\eta_{2.5}^{-8/3}n^{-1/3}, & k=0, \\ 0.02\,{\rm s}E_{\rm K,53}\eta_{2.5}^{-4}A_{35.5}^{-1}, & k=2. \end{cases} \quad (1)$$

The deceleration radius can be written as

$$R_{\rm dec} = \left(\frac{3-k}{4\pi}\frac{E_{\rm K,iso}}{\eta^2 A m_p c^2}\right)^{1/(3-k)} = \begin{cases} 6\times10^{16}\,{\rm cm}E_{\rm K,53}^{1/3}\eta_{2.5}^{-2/3}n^{-1/3}, & k=0, \\ 2\times10^{14}\,{\rm cm}E_{\rm K,53}\eta_{2.5}^{-2}A_{35.5}^{-1}, & k=2. \end{cases} \quad (2)$$

Before the deceleration time, the central engine is still working. The mass ejected later catches up with the earlier ones, and Γ can be simplified as the bulk Lorentz factor of these materials combination. It can also be believed that the bulk Lorentz factor in the very beginning is too low for majority of high-energy gamma rays to escape. Only when

$\tau_{\gamma\gamma} < 1$, the bulk Lorentz factor is large enough to radiate almost completely without taking absorption into account. In the following analytical calculations, we assume that the self-similar condition is established after the deceleration time.

3.1.2. Lower Limits of the Lorentz Factor

Since the highest energy photons can place a tight constraint on the Lorentz factor of the ejecta via the pair-production threshold, the optical depth for photon annihilation is crucial to the observed fluence. With the photon energy of the Band function's turning point $E_{\rm b} = (\alpha_{\rm band} - \beta_{\rm band})/(2 + \alpha_{\rm band})E_{\rm p}$, factor $f \approx (\beta_{\rm band} - 2)(F_h/T_{90}){E_{\rm b}}^{\beta_{\rm band}-2}$, and the threshold of the photon observed $E_{\rm max,an} = (\Gamma m_e c^2)^2/[(1+z)^2 E_{\rm max}]$, while in the local frame, the total photon number whose energy is larger than $E'_{\rm max} = E_{\rm max}(1+z)$ can be estimated as $N_{>{\rm E_{max,an}(1+z)}} \approx 4\pi D_L^2 f t E_{\rm max,an}^{1-\beta}/[(1+z)^2(\beta-1)]$. Therefore, the pair-production threshold for photons with energy can be estimated as

$$\tau_{\gamma\gamma}(E'_{\rm max}) = \frac{(11/180)\sigma_T N_{>{\rm E_{max,an}(1+z)}}}{4\pi R^2} = \frac{11\sigma_T}{180R^2}(\frac{D_L}{1+z})^2 \frac{ft}{\beta-1}[\frac{E_{\rm max}(1+z)^2}{(\Gamma m_e c^2)^2}]^{\beta_{\rm band}-1} \quad (3)$$

where $\beta_{\rm band}$, $\alpha_{\rm band}$ and E_p are the indices and peak energy of the Band function respectively (Band et al. 1992), $E_{\rm max}$ is the observed maximum photon energy, m_e is the electron mass, σ_T is the Thomson cross section, F_h represents the time-integrated flux of higher band ($1-10^4$keV in Zhang et al. (2010)) during the prompt emission, and the luminosity distance $D_L = [(1+z)c/H_0]\int_0^z [\Omega_m(1+z)^3 + \Omega_k(1+z)^2 + \Omega_\Lambda]^{-1/2}dz$ (here we adopt a standard ΛCDM cosmology with $H_0 = 71{\rm kms^{-1}Mpc^{-1}}$, $\Omega_m = 0.27$, $\Omega_k = 0.0$, $\Omega_\Lambda = 0.73$ (Spergel et al. 2007)).

As we mentioned above, the optical depth at the deceleration time should be thin, so we can estimate the lower limit of Lorentz factor at this turning point from equation(3).

3.1.3. In the Density-Jump Surrounding

Because of the association of long GRBs with star forming regions, it is highly possible that massive stars are still embedded in a cloud when giving birth to GRBs. Low density bubbles are created by stellar winds from GRB progenitors, whose sizes and densities strongly depend on the initial ambient density. Therefore, a density jump occurs at the boundary between the wind bubble and the outer cloud, which may result in a bump/flare and shallow decay of the light curve during the later period (Tam et al. 2005).

From the moment $t_{\rm break}$ at which the blast wave reaches the boundary, to the termination when it comes out into the interstellar medium at $t_{\rm end}$, the number density of the medium changes as

$$n = AR^{-k} = \begin{cases} 3\times10^{35}A_{35.5}R^{-2}, & R \le R_{\rm break}, \\ 3\times10^{35}[1+\frac{\log R-\log R_{\rm break}}{\log R_{\rm end}-\log R_{\rm break}}(\xi-1)]A_{35.5}R_{\rm break}^{-2}, & R_{\rm break} \le R \le R_{\rm end}, \\ n_{\rm after} = 3\times10^{35}\xi A_{35.5}R_{\rm break}^{-2}, & R \ge R_{\rm end}, \end{cases} \tag{4}$$

where ξ is the ratio of the number density in front of and behind the jump.

It has been usually assumed that the afterglow emission from the blast wave is nearly adiabatic (Mészáros & Rees 1997; Sari et al. 1998), so the total kinetic energy of the relativistic shock is constant. However, if we take the energy loss into consideration, the radiation efficiency of the blast wave can be given by (Wu et al. 2005a)

$$\varepsilon = \begin{cases} \epsilon_e, & \nu_c \le \nu_m, \\ \epsilon_e(\frac{\nu_m}{\nu_c})^{(p-2)/2}, & \nu_m \ge \nu_c. \end{cases} \tag{5}$$

In such a situation, energy loss is significant in the fast cooling and gradually dwindle to the quasi-adiabatic case (i.e., the slow cooling phase).

Hereafter, a denotation $m = (3-k)/(1-\varepsilon)$ can analytically result in the bulk Lorentz factor evolution,

$$\Gamma = \begin{cases} \eta(\frac{t}{t_{\rm dec}})^{s}, & t \le t_{\rm dec}, \\ \eta(\frac{t}{t_{\rm dec}})^{-m/[2(m+1)]}, & t \ge t_{\rm dec}. \end{cases} \tag{6}$$

Consequently, the Doppler factor becomes $\mathcal{D}= \frac{1}{\Gamma(1-\beta cos\theta)} = \frac{2\Gamma}{1+\Gamma^2\theta^2} \sim 2\Gamma$ (where θ is the emitting latitude angle).

When the blast shock reaches the density boundary, the observed light curve will not behave as an abrupt jump but a smooth rise or plateau instead, due to the curvature effect (Fenimore et al. 1996; Kumar & Panaitescu 2000). Although this is trifle to be accomplished in analytic modeling, a simplified power law distribution of medium density in the period of $t_{\rm break} \sim t_{\rm end}$ can account for the same light curve feature (See Fig 1a). Succeedingly, the blast wave radius can be written as

$$R = \frac{2(4-k)\Gamma^2 ct}{1+z} = \begin{cases} R_{\rm dec}(\frac{t}{t_{\rm dec}})^{2s+1}, & t \le t_{\rm dec}, \\ R_{\rm dec}(\frac{t}{t_{\rm dec}})^{(1-\varepsilon)/(4-k-\varepsilon)}, & t \ge t_{\rm dec}. \end{cases} \tag{7}$$

3.2. Radiation

In the comoving frame, with an electronic fraction ϵ_e and magnetic fraction ϵ_B of the post-shock thermal energy density, which may either vary or not with different media, the magnetic field intensity $B = \Gamma(32\pi\epsilon_B n m_p c^2)^{1/2}$. The cooling, minimum, and maximum electron Lorentz factors are $\gamma_{e,c} = 6\pi m_e c(1+z)/[\sigma_T B^2 \Gamma t(1+Y)]$, $\gamma_{e,\min} = \epsilon_e[(p-2)/(p-1)](m_p/m_e)\Gamma$, and $\gamma_{e,\max} = 10^8/\sqrt{B(1+Y)}$, while the synchrotron characteristic frequencies ν_c, $\nu_{\min}$, $\nu_{\max}$ can be calculated by $\nu_i = \gamma_{e,i}^2 \mathcal{D}[eB/(2\pi(1+z)m_e c)]$ (where $i = c, \min, \max$), where Y is the Compton factor for electrons with the Lorentz factor γ_e, defined as the ratio of the self-inverse Compton (SSC) to synchrotron luminosity, and can be preliminarily analytically expressed as (Sari & Esin 2001)

$$Y(\gamma_e) \equiv \frac{P_{SSC}(\gamma_e)}{P_{syn}(\gamma_e)} \approx \begin{cases} \sqrt{\frac{1}{4} + \frac{\epsilon_e}{\epsilon_B}} - 0.5, & \gamma_{e,c} \leq \gamma_{e,\min}, \\ \sqrt{\frac{1}{4} + \frac{\epsilon_e}{\epsilon_B}(\frac{\gamma_{e,\min}}{\gamma_{e,c}})^{p-2}} - 0.5, & \gamma_{e,c} \geq \gamma_{e,\min}. \end{cases} \tag{8}$$

The total number of shocked accelerated electrons $N_e = 4\pi n R^3/(3-k)$. The peak spectral power of a single electron is $P_{\nu,\max} = \sigma_T m_e c^2 \mathcal{D} B/(3e)$, and the peak flux density at certain time of the afterglow is $F_{\nu,\max} = (1+z)N_e P_{\nu,\max}/(4\pi {D_L}^2)$.

For a lower energy band (e.g., radio), synchrotron self-absorption may play a crucial role. The self-absorption optical depth $\tau_{\nu,m}$ or $(\tau_{\nu,c})$, according to the definition $\tau_\nu = 1$, becomes $\tau_{\nu,m} = \frac{c_0(p-1)}{(3-k)}\frac{enR}{B{\gamma_m}^5}$ and $\tau_{\nu,c} = \frac{c_0}{(3-k)}\frac{enR}{B{\gamma_c}^5}$, where $c_0 \approx 10.4[(p+2)/(p+2/3)]$ (Wu et al. 2005). Succeedingly, the self-absorption frequency ν_a can be written as

$$\nu_a = \begin{cases} \tau_{\nu,l}^{3/5}\nu_l, & \tau_{\nu,l} < 1, \\ \tau_{\nu,l}^{2/(p+4)}\nu_l, & 1 \leq \tau_{\nu,l} < (\nu_h/\nu_l)^{(p+4)/2}, \\ \tau_{\nu,l}^{2/(p+5)}(\frac{\nu_h}{\nu_l})^{1/(p+5)}\nu_l, & (\nu_h/\nu_l)^{(p+4)/2} \leq \tau_{\nu,l} < (\frac{\nu_{\max}}{\nu_l})^{(p+5)/2}(\frac{\nu_l}{\nu_h})^{1/2}. \end{cases} \tag{9}$$

Then, the SSA power-law light curve yields (Sari & Esin 2001)

$$F_\nu = F_{\nu,max} \begin{cases} (\frac{\nu_a}{\nu_l})^{1/3}(\frac{\nu}{\nu_a})^2, & \nu \leq \nu_a, \\ (\frac{\nu}{\nu_l})^{1/3}, & \nu \leq \nu_l, \\ (\frac{\nu}{\nu_l})^{-(q-1)/2}, & \nu_l \leq \nu \leq \nu_h, \\ (\frac{\nu_h}{\nu_l})^{-(q-1)/2}(\frac{\nu}{\nu_h})^{-p/2}, & \nu \geq \nu_h. \end{cases} \tag{10}$$

Here $\nu_l = \min(\nu_m, \nu_c)$, $\nu_h = \max(\nu_m, \nu_c)$. q= 2 when $\nu_c < \nu_m$, while $\nu_c > \nu_m$, $q = p$.

It is noted that before the central engine ceases, the annihilation effect of high-energy photons can affect their flux, so the observed flux can be estimated as $F_{\mathrm{ob},\nu} = F_\nu(1 - e^{-\tau_{\gamma\gamma}})/\tau_{\gamma\gamma}$. After the blast wave enters the self-similar phase, $F_{\mathrm{ob},\nu} = F_\nu$.

For a high energy band, synchrotron self-Compton (SSC) radiation might contribute to the observed flux, the characteristic frequencies $\nu_{IC,c}$, $\nu_{IC,\min}$, $\nu_{IC,\max}$, $F_{IC,\nu,\max}$ can be calculated by $\nu_{IC,i} = 2\nu_i\gamma_{e,i}^2$ (where $i = c, \min, \max$), and $F_{IC,\nu,\max} = (14/45)\sigma_T RnF_{\nu,\max}$. Thus the SSC power-law light curve yields (Gupta & Zhang 2007)

$$F_{\nu,IC} = F_{IC,max}\begin{cases} (\frac{\nu}{\nu_{IC,l}})^{1/3}, & \nu \leq \nu_{IC,l}, \\ (\frac{\nu}{\nu_{IC,l}})^{-(q-1)/2}, & \nu_{IC,l} \leq \nu \leq \nu_{IC,h}, \\ (\frac{\nu_{IC,h}}{\nu_{IC,l}})^{-(q-1)/2}(\frac{\nu}{\nu_{IC,h}})^{-p/2}, & \nu_{IC,h} \leq \nu \end{cases} \tag{11}$$

Here $\nu_{IC,l} = \min(\nu_{IC,m}, \nu_{IC,c})$, $\nu_{IC,h} = \max(\nu_{IC,m}, \nu_{IC,c})$. $q = 2$ when $\nu_{IC,c} < \nu_{IC,m}$, while $\nu_{IC,c} > \nu_{IC,m}$, $q = p$. It is noted that the high-energy photon may be in the Klein-Nishina regime, which calls for another characteristic frequency, $\nu_{KN} = \gamma^2 {m_e}^2 c^4/[h^2 \max(\nu_m, \nu_c)]$ with h being the Plank constant. Hereafter, equation (11) should be amended as $F_{\nu,IC} = \kappa F_{\nu_{KN},IC}$, where κ is the correction factor and $\kappa = 1$ when $\nu_{KN} > \nu$, while $\kappa = (\nu/\nu_{KN})^{-(p+1)}$ when $\nu_{KN} \leq \nu$.

Hence, the analytical expression in equation (8) is so coarse that it may be suppressed by the Klein-Nishina factor κ even when ϵ_e/ϵ_B is large.

In the case of a jet, a simple assumption is that the jet decelerates without sideways expansion. After the jet break time t_{jet} at which the jet angle $\theta_j \sim 1/\Gamma$ (where the jet axis is assumed to be along the line of sight), the observed flux $F_{\nu,\mathrm{jet}} = F_\nu(t/t_{jet})^{(3-k)/(4-k)}$.

Comparing the flux density estimated analytically above with the observational multi-band values, certain physical parameters can be constrained. Whether the parameter space is reasonable or not can on some extent verify the feasibility of our external shock model.

4. Fitting Results

4.1. Constraints on Parameters

The lower limit of the Lorentz factors for GRB080916C, GRB090902B and GRB090926A calculated from §3.2 provides a constraint on the initial bulk Lorentz factor η at the deceleration time (shown in Table 1). Based on the analytical model we mentioned above, our procedure of further narrowing down the physical parameter space in the self-similar phase includes the following steps:

In the wind environment:

(1) According to the expression of $F_\nu \propto t^{-\alpha}\nu^{-\beta}$ in different spectral regimes given by

Wu et al. (2005) and the observed high-energy, X-ray and optical temporal and spectral indices, (p, ε) can be roughly estimated (see Table 2).

(2) For simplicity, $\varepsilon \approx \epsilon_e$ in the fast cooling regime and then ε decays slowly (where we denote t_{cm} as the time when $\nu_c = \nu_m$, and obtain that ε decays as $\varepsilon \sim \epsilon_e (t/t_{cm})^{2-p}$ in the slow cooling regime (i.e., setting j as the temporal index of Γ after t_{cm}, $\Gamma \propto t^j$, then $\nu_m \propto t^{(j-1)}$ and $\nu_c \propto t^{(j+1)}$, and equation (5) provides $\epsilon \propto \epsilon_e (\nu_m/\nu_c)^{(p-2)/2} \propto t^{(2-p)}$, independent of j).

(3) Because of the definition for deceleration time (see equation (1) and (2)), η can be expressed with $E_{\rm K,iso}$ and n (or $A_{35.5}$).

(4) Hereafter the free parameters are $E_{\rm K,iso}$, $\epsilon_{\rm B}$, and n (or $A_{35.5}$). The observed flux density in different wavebands (radio, optical, X-ray, >100 MeV) can be combined and eventually simultaneously be solved. In this paper, the temporal indices of the X-ray and optical light curves concurrently evolve according to equation (10) and thus ϵ_B can therefore be expressed with $E_{\rm K,iso}$ and n (or $A_{35.5}$).

(5) To justify whether the early high energy LAT photons come from the same region as the late afterglow, what we need to do is to replace ϵ_B in the form of $E_{\rm K,iso}$ and n (or A) from step (4). If no solution is found in the range of (10^{45} ergs $\leq E_{\rm K,iso} \leq 10^{58}$ ergs and $10^{-10} \leq A_{35.5} \leq 10^5$), the >100 MeV photons may come from the other component, vise vesa.

The rising index s of the Lorentz factor during the prompt emission and the ratio ξ of the wind and homogeneous medium density are two free parameters for fitting. In addition, ϵ_e and ϵ_B at early and late times may have slight changes, which can also be legally adjusted in practise.

4.2. Best Fittings

We put the above procedure into operation, and best fitting parameters are shown in Table 3. The evolutions of characteristic frequencies for each burst are expected as follows. Here our LAT data are taken from Zhang et al. (2010) and X-ray data were reported by Swift (Evans et al. 2007; Evans et al. 2009).

4.2.1. GRB080916C

Our optical photometry of this burst is taken from Greiner et al. (2009). First of all, if the X-ray and optical afterglow shares the same source as the high-energy photons de-

tected by LAT, their spectral indices $\beta_{ob,x} = 0.50 \pm 0.16$ and $\beta_{ob,opt} = 0.38 \pm 0.02$ should be consistent with the GeV $\alpha_{ob,LAT} = 1.2 \pm 0.2$ and $\beta_{ob,LAT} = 1.1 \pm 0.1$. According to the analytical expression from Wu et al. (2005), before the blast wave reaches the density jump, GeV photons at early decaying times are probably in one of the regimes: (1) $\nu_{LAT} \geq \nu_{\rm min} \geq \nu_c$, (2) $\nu_{LAT} \geq \nu_c \geq \nu_{\rm min}$, while the lower energy bands later may lie in either (3) $\nu_c \geq \nu_{X,opt} \geq \nu_{\rm min}$ or (4) $\nu_{X,opt} \geq \nu_c \geq \nu_{\rm min}$. Therefore, the flux density may be proportional to (1) $t^{-[3p-2-(p-2)\varepsilon]/[2(2-\varepsilon)]}\nu^{-p/2}$, (2) $t^{-[3p-2-(p-2)\varepsilon]/[2(2-\varepsilon)]+(p-2)/(4-p)}\nu^{-p/2}$, (3) & (4) $t^{-[3p-1-(p-1)\varepsilon]/[2(2-\varepsilon)]}\nu^{-(p-1)/2}$, respectively, which is preliminarily valid when $2.0 \leq p \leq 2.3$ and $0 < \epsilon_e \leq 0.48$.

Consequently, the peak of the LAT light curve lying at $t_{dec} \sim 5$s can be considered as the deceleration time of this burst. Therefore, equation (1) and equation (2) lead to the relationship among the isotropic kinetic energy $E_{\rm K,55}$, the bulk Lorentz factor η_3, and the wind parameter $A_{35.5}$ at the very moment: $\eta_3 \sim [E_{\rm K,55}/(80.2A_{35.5})]^{1/4}$.

Subsequently, when the blast wave is embedded in the wind bubble during the early period, if the LAT photons are in regime (1) or (2), the flux density can be estimated as $F_{syn,\nu_{LAT}} = (\nu_m/\nu_c)^{-1/2}(\nu_{LAT}/\nu_m)^{-p/2}F_{max,\nu_{LAT}}$ or $F_{syn,\nu_{LAT}} = (\nu_c/\nu_m)^{-(p-1)/2}(\nu_{LAT}/\nu_c)^{-p/2}F_{max,\nu_{LAT}}$, respectively. At the late times when the blast wave is about to crush out of the boundary, if the case of lower energy is in (3) or (4), the expected flux density should be $F_{syn,\nu_{X,opt}} = (\nu_{X,opt}/\nu_m)^{-(p-1)/2}F_{\rm max,\nu_{X,opt}}$ or $F_{syn,\nu_{X,opt}} = (\nu_c/\nu_m)^{-(p-1)/2}(\nu_{X,opt}/\nu_c)^{-p/2}F_{\rm max,\nu_{X,opt}}$, accordingly. Furthermore, under certain circumstances, if the Y factor is large enough, lower-energy photons may be boosted into the higher band (by means of inverse Compton scattering) contributing to the detected flux density. Hence, our calculation should take this component into account, which can be written in the form of equation (11).

Next we test four cases of regime combinement, e.g., (1)+(3), (1)+(4), (2)+(3), and (2)+(4), and found that only case (2)+(3) is favored and the best-fit to the observed data gives $p = 2.32$ and $\epsilon_{e,0} = 0.3$. With $E_{\rm K,55}, \epsilon_{B,0}$ and $A_{35.5}$ leaving uncertain, the characteristic frequencies and flux density at two typical times are given as follows: In the self-similar phase with the wind bubble, at t=13s,

$$\nu_{KN} = 1.12 \times 10^{35}\,{\rm Hz} A_{35.5}^{3/2}\epsilon_{B,0}^{3/2}(1+Y)^2, \tag{12}$$

and $\min(\nu_{IC,c}, \nu_{IC,m}) > \nu_{LAT} > \max(\nu_c, \nu_m)$,

$$\nu_{IC,c} = 5.57 \times 10^{8}\,{\rm Hz} E_{\rm K,55} A_{35.5}^{-9/2}\epsilon_{B,0}^{-7/2}(1+Y)^{-4} > 1\,{\rm GeV}, \tag{13}$$

$$\nu_{IC,\rm min} = 1.40 \times 10^{30}\,{\rm Hz} E_{\rm K,55} A_{35.5}^{-1/2}\epsilon_{B,0}^{1/2} > 1\,{\rm GeV}, \tag{14}$$

$$\nu_c = 1.03 \times 10^{10}\,{\rm Hz} E_{\rm K,55}^{1/2} A_{35.5}^{-2}\epsilon_{B,0}^{-3/2}(1+Y)^{-2} < 1\,{\rm GeV}, \tag{15}$$

$$\nu_{min} = 5.18 \times 10^{20}\,\mathrm{Hz} E_{\mathrm{K},55}^{1/2} \epsilon_{B,0}^{1/2} < 1\,\mathrm{GeV}. \tag{16}$$

The observed flux density coming from synchrotron emission and IC upscattered photons in the external shock model are calculated by

$$F_{syn,1\mathrm{GeV}} = 7.01\,\mu\mathrm{Jy} E_{\mathrm{K},55}^{27/25} \epsilon_{B,0}^{2/25} (1+Y)^{-1}, \tag{17}$$

$$F_{IC,1\mathrm{GeV}} = 9.79 \times 10^{-1} \mu\mathrm{Jy} E_{\mathrm{K},55}^{-1/3} A_{35.5}^{8/3} \epsilon_{B,0}^{1/3} \kappa, \tag{18}$$

whose summation is equal to the observed value under consideration of the Klein-Nishina suppression factor κ,

$$F_{syn,1\mathrm{GeV}} + F_{IC,1\mathrm{GeV}} \sim 0.83\,\mu\mathrm{Jy}. \tag{19}$$

As for the X-ray band and WH filter, at $t = 1.01 \times 10^5$ s, $\nu_c > 1\mathrm{keV} > 3\,\mathrm{eV} > \nu_m$,

$$\nu_c = 1.18 \times 10^{20}\,\mathrm{Hz} E_{\mathrm{K},55}^{1/2} A_{35.5}^{-2} \epsilon_{B,0}^{-3/2} (1+Y)^{-2} > 1\,\mathrm{keV} > 3\,\mathrm{eV}, \tag{20}$$

$$\nu_{\mathrm{min}} = 1.62 \times 10^{15}\,\mathrm{Hz} E_{\mathrm{K},55}^{1/2} \epsilon_{B,0}^{1/2} < 3\,\mathrm{eV} < 1\,\mathrm{keV}, \tag{21}$$

and their flux density should be around the observed value in the case of the same source shared as higher band,

$$F_{syn,X} = 6.05 \times 10^4\,\mu\mathrm{Jy} E_{\mathrm{K},55}^{5/6} A_{35.5} \epsilon_{B,0}^{5/6} \sim 7.73 \times 10^{-2}\,\mu\mathrm{Jy}, \tag{22}$$

$$F_{syn,opt} = 6.98 \times 10^6\,\mu\mathrm{Jy} E_{\mathrm{K},55}^{5/6} A_{35.5} \epsilon_{B,0}^{5/6} \sim 6.2\,\mu\mathrm{Jy}. \tag{23}$$

The best fitting yields $E_{\mathrm{K},55} = 3.16$, $A_{35.5} = 10^{-1}$, $\epsilon_{B,0} = 1.31 \times 10^{-6}$, and $\eta_3 = 0.8$. As the result shown in Fig 2: before the deceleration time, the bulk Lorentz factor of the swept blast wave increases with $s = 0.5$, t_{cm} occurs at ~ 0.9s and the electrons are fast cooling, then deceleration begins since ~ 5 s, the density jump is expected around $10^{5.3} - 10^{5.6}$ s (i.e., 7.36×10^{18} cm). After breaking out to the interstellar medium, the surrounding density is around $1.27 \times 10^{-3}\mathrm{cm}^{-3}$. During the whole period, Y$\ll$1, which indicates that IC is strongly suppressed by the Klein-Nishina effect.

4.2.2. GRB090902B

Along with the LAT and XRT data mentioned above, our optical photometry here is taken from Pandey et al. (2010), as well as the 4.8GHz data reported by the WSRT (van der Horst et al. 2009). With the assumption that late X-ray, optical and radio afterglow and the early LAT photons originate from the same region, their spectral indices $\beta_{ob,x} = 0.90 \pm 0.13$ and $\beta_{ob,opt} = 0.76 \pm 0.07$ should be consistent with the GeV, $\alpha_{ob,LAT} = 1.5 \pm 0.1$.

The same as the above analysis, GeV may be in one of the (1)/(2) and lower energy photons may be in one of the (3)/(4) regimes, respectively, which result in the plausible light curve and spectrum similar to the above case. Therefore, roughly speaking, $2.3 \leq p \leq 2.4$ and $0.17 \leq \epsilon_e \leq 0.43$ are the available region.

Although the peculiar "soft-hard" spectral evolution seems tricky in the prompt emission phase, its duration is so short ($T_0 - T_0 + 10$ s) and it ends before the deceleration time (Zhang et al. 2010), which, is understandable in the frame of structured ejecta acceleration (we will discuss it in §5), so the external shock model is still applicable. In addition, although a 33 GeV photon was detected at 82 s after the trigger, we consider the 11.2 GeV photon at ~ 10 s as the highest energy photon of estimation for the lower Lorentz factor because the arrival time of the 33GeV photon is far beyond the prompt emission phase and may not merely be attributed from the external shock but some other origins.

The turning point of the LAT light curve occurs at $\sim$7 s. This indicates that a relationship among $E_{\rm K,55}$, η_3, and $A_{\star,35.5}$ becomes $\eta_3 \sim [E_{\rm K,55}/(168.6 A_{35.5})]^{1/4}$.

Similar to analytical solutions of GRB080916C we mentioned above, characteristic frequencies of the photons observed by LAT and later multiband (X-ray, optical, radio) afterglow can be estimated. Additionally, when we come to the radio band, SSA may be crucial. Afterward, check every case and find (2)+(3) would be the suitable regime, and deliberate fit favors when $p = 2.3$ and $\epsilon_{e,0} = 0.2$. Thus, the characteristic frequencies and estimated flux density can be written with model parameters ($E_{\rm K,55}, \epsilon_{B,0}$ and $A_{\star,35.5}$) as follows:

At a typical LAT decaying time (i.e., $t = 10$ s), GeV photons lie between IC and synchrotron frequencies,

$$\nu_{KN} = 4.05 \times 10^{34} {\rm Hz} {\rm A}_{35.5}^{3/2} \epsilon_{\rm B,0}^{3/2} (1+{\rm Y})^2, \tag{24}$$

and $\min(\nu_{IC,m}, \nu_{IC,c}) > \nu_{LAT} > \max(\nu_m, \nu_c)$,

$$\nu_{IC,c} = 2.40 \times 10^9\,{\rm Hz} E_{\rm K,55} A_{35.5}^{-9/2} \epsilon_{B,0}^{-7/2} (1+Y)^{-4} > 1\,{\rm GeV}, \tag{25}$$

$$\nu_{IC,\rm min} = 2.01 \times 10^{30}\,{\rm Hz} E_{\rm K,55} A_{35.5}^{-1/2} \epsilon_{B,0}^{1/2} > 1\,{\rm GeV}, \tag{26}$$

$$\nu_c = 2.44 \times 10^{10}\,{\rm Hz} E_{\rm K,55}^{1/2} A_{35.5}^{-2} \epsilon_{B,0}^{-3/2} (1+Y)^{-2} < 1\,{\rm GeV}, \tag{27}$$

$$\nu_{\rm min} = 7.05 \times 10^{20}\,{\rm Hz} E_{\rm K,55}^{1/2} \epsilon_{B,0}^{1/2} < 1\,{\rm GeV}. \tag{28}$$

This regime may lead to the accumulated flux density as high as

$$F_{syn,1{\rm GeV}} = 50.1\,\mu{\rm Jy} E_{\rm K,55}^{43/40} \epsilon_{B,0}^{3/40} (1+Y)^{-1}, \tag{29}$$

$$F_{IC,1{\rm GeV}} = 2.56\,\mu{\rm Jy} E_{\rm K,55}^{-1/3} A_{35.5}^{8/3} \epsilon_{B,0}^{1/3} \kappa, \tag{30}$$

The total flux density at 1 GeV is

$$F_{syn,1\mathrm{GeV}} + F_{IC,1\mathrm{GeV}} \sim 1.59\,\mu\mathrm{Jy}. \tag{31}$$

The photons in X-ray and optical bands (R-,U-,V-,B-,NIR) were observed at later times (typically $t = 104534$ s). These photons lie between the cooling frequency and minimum frequency, $\nu_c > 1\,\mathrm{keV} > \nu_R > \nu_m$,

$$\nu_c = 5.00 \times 10^{12}\,\mathrm{Hz} E_{\mathrm{K},55}^{1/2} A_{35.5}^{-2} \epsilon_{B,0}^{-3/2} (1+Y)^{-2} > 1\,\mathrm{keV} > R - \mathrm{band}, \tag{32}$$

$$\nu_{\min} = 1.52 \times 10^{15}\,\mathrm{Hz} E_{\mathrm{K},55}^{1/2} \epsilon_{B,0}^{1/2} < R - \mathrm{band} < 1\,\mathrm{keV}. \tag{33}$$

The corresponding flux densities are calculated by

$$F_{syn,X} = 2.00 \times 10^{5}\,\mu\mathrm{Jy} E_{\mathrm{K},55}^{33/40} A_{35.5} \epsilon_{B,0}^{33/40} \sim 0.16\,\mu\mathrm{Jy}, \tag{34}$$

$$F_{syn,R} = 1.22 \times 10^{7}\,\mu\mathrm{Jy} E_{\mathrm{K},55}^{33/40} A_{35.5} \epsilon_{B,0}^{33/40} \sim 9.0\,\mu\mathrm{Jy}. \tag{35}$$

The best fitting requires $E_{\mathrm{K},55} = 0.8$, $A_{35.5} = 10^{-2}$, $\epsilon_{B,0} = 10^{-4}$, and $\eta_3 = 0.8$. Fig 1. shows the circumburst density, radius, Y factor and characteristic electron Lorentz factor evolution under such a parameter space. Fig 3 shows the spectrum and light curve fitting. Before the deceleration time, the bulk Lorentz factor of the blast wave increase with a slope of $s = 0.5$. The shock-accelerated electrons are cooling fast early before ~ 0.1 s, density jump is estimated around $10^{5.1} - 10^{6}$ s (i.e., at radius of 1.64×10^{19} cm). After breaking out to the interstellar medium, the surrounding density is as low as $2.21 \times 10^{-5}\,\mathrm{cm}^{-3}$. These parameters are consistent with the radio light curve except for the first data and is reliable when the jet break takes place nearly at the same time. We find that the jet angle is 0.04 rad and collimation-corrected energy is $E_{jet} \sim 3 \times 10^{51}$ ergs. During this whole period, $Y \ll 1$, which indicates that SSC makes a little effect due to the Klein-Nishina suppression (As a matter of fact, ν_{KN} is so low that only until $\sim 10^4$s does it higher than $\nu_{IC,\min}$).

4.2.3. GRB090926A

V band and R band data of this burst are taken from Swenson et al. (2010) and Rau et al. (2010), respectively. Our analysis procedure is the same as mentioned above. Due to the hypothesis of the same source, the temporal index of the LAT photons $\alpha_{ob,LAT} = 2.17 \pm 0.14$, should be consistent with the spectral indices $\beta_{ob,x} = 1.12 \pm 0.13$ and $\beta_{ob,opt} = 1.03 \pm 0.05$. This leads to a fairly broad plausible range for p and ϵ_e. However, since the light curve after the density jump is a little bit steeper than the early part, ϵ_e should not

deviate too much from the typical value (i.e., 1/3, otherwise, the decrease of loss efficiency will cause the decaying slope much shallower), whereas the decay of LAT is steep, which requires a large p (i.e., 3.0). Besides, in the afterglow phase, we can reasonably believe that the first flare at $70-95$ ks comes from an interaction of the blast wave and density jump. The second "flare" may come from late energy injection or another density jump, and in this paper, we smooth it as the simple power law.

Because the deceleration time is estimated as $\sim$ 16 s, η_3 can be written by $\eta_3 \sim [E_{\rm K,55}/(334A_{35.5})]^{1/4}$. Four cases (LAT photons in regime (1) or (2) as well as lower later ones in (3) or (4) regime) have been tested and deliberate fit favors (2)+(3) when $p = 3.0$ and $\epsilon_{e,0} = 0.35$. Thus the characteristic frequencies and estimated flux density can be written with uncertain $E_{\rm K,55}, \epsilon_{B,0}$ and $A_{\star,35.5}$ as follows: at $t = 36$ s, the LAT light curve is in the decaying phase,

$$\nu_{KN} = 1.36 \times 10^{34}\,{\rm Hz} A_{35.5}^{3/2}\epsilon_{B,0}^{3/2}(1+Y)^2 \tag{36}$$

and $\min(\nu_{IC,m}, \nu_{IC,c}) > \nu_{LAT} > \max(\nu_c, \nu_m)$, which yields

$$\nu_{IC,c} = 2.29 \times 10^{10}\,{\rm Hz} E_{\rm K,55} A_{35.5}^{-9/2}\epsilon_{B,0}^{-7/2}(1+Y)^{-4} > 1\,{\rm GeV}, \tag{37}$$

$$\nu_{IC,\rm min} = 3.66 \times 10^{30}\,{\rm Hz} E_{\rm K,55} A_{35.5}^{-1/2}\epsilon_{B,0}^{1/2} > 1\,{\rm GeV}, \tag{38}$$

$$\nu_c = 3.96 \times 10^{10}\,{\rm Hz} E_{\rm K,55}^{1/2} A_{35.5}^{-2}\epsilon_{B,0}^{-3/2}(1+Y)^{-2} < 1\,{\rm GeV}, \tag{39}$$

$$\nu_{\rm min} = 5.02 \times 10^{20}\,{\rm Hz} E_{\rm K,55}^{1/2}\epsilon_{B,0}^{1/2} < 1\,{\rm GeV}, \tag{40}$$

and the contribution from synchrotron emission and SSC can be calculated by

$$F_{syn,\rm 1GeV} = 5.58\,\mu{\rm Jy} E_{\rm K,55}^{5/4}\epsilon_{B,0}^{1/4}(1+Y)^{-1}, \tag{41}$$

$$F_{IC,\rm 1GeV} = 0.49\mu{\rm Jy} E_{\rm K,55}^{-1/3} A_{35.5}^{8/3}\epsilon_{B,0}^{1/3}\kappa. \tag{42}$$

This flux density should be suppressed by κ under consideration of the Klein-Nishina effect.

$$F_{syn,\rm 1GeV} + F_{IC,1GeV} \sim 0.37\mu{\rm Jy}. \tag{43}$$

Since the lower energy detector started in operation at $t = 53127$ s, ν_c >1keV>V band> ν_m may be a reasonable frequency regime,

$$\nu_c = 6.67 \times 10^{18}\,{\rm Hz} E_{\rm K,55}^{1/2} A_{35.5}^{-2}\epsilon_{B,0}^{-3/2}(1+Y)^{-2} > 1\,{\rm keV} > (R-, V-){\rm band}, \tag{44}$$

$$\nu_{\rm min} = 1.81 \times 10^{16}\,{\rm Hz} E_{\rm K,55}^{1/2}\epsilon_{B,0}^{1/2} < (R-, V-){\rm band} < 1\,{\rm keV}, \tag{45}$$

where the X-ray and optical flux density becomes

$$F_{syn,X} = 5.95 \times 10^4\,\mu{\rm Jy} E_{\rm K,55} A_{35.5}\epsilon_{B,0} \sim 0.33\mu{\rm Jy}, \tag{46}$$

$$F_{syn,R,V} = 1.84 \times 10^8\,\mu\mathrm{Jy} E_{\mathrm{K},55} A_{35.5} \epsilon_{B,0} \sim 1.02 \times 10^2\,\mu\mathrm{Jy}. \quad (47)$$

When $E_{\mathrm{K},55} = 2.74$, $A_{35.5} = 10^{-1}$, $\epsilon_{B,0} = 4.5 \times 10^{-6}$, and $\eta_3 = 0.55$, fitting seems plausible. Before the deceleration time, the Lorentz factor of the blast wave increases with a slope of $s = 0.2$, $t_{cm} \sim 3$ s and from $\sim 16s$ significant deceleration appears. The blast wave enters the ISM around $10^{4.8} - 10^{4.9}$ s (i.e., at radius of 7.37×10^{18} cm). The medium density surrounding the bubble is $1.38 \times 10^{-3}\,\mathrm{cm}^{-3}$. In this whole period, $Y \ll 1$, SSC therefore does not quite obviously impact upon the light curve.

4.3. Analysis of Results

Table 3 shows all the best fit parameters for the above three GRBs. Common results can be found:

(1) The bulk Lorentz factor of structured ejecta increases as a power law with small index (≤ 0.5), indicating that the central engine is very likely to be the core collapse of a massive star (we will discuss it in §5). Our model implies that the central object would keep on accreting matter even after the LAT triggers.

(2) The remaining isotropic kinetic energy of the fireball after the prompt emission are all $10^{54} \sim 10^{55}$ ergs, $\sim 60\% - 90\%$ of the total, indicating a little bit more energy emission in the afterglow under consideration of energy loss. This is because t_{cm} occurs before the deceleration time for all the three GRBs and the following dynamics could be considered as being quasi-adiabatic. As a matter of fact, ϵ_e in our sample fittings is $\leqslant 2/3$, which meets the requirement of radiation efficiency related to the analytic procedure from Wu et al. (2005). Practically, slow cooling of electrons starts before the deceleration time, and a jet break appears much later, so Wu's spherical-like solution is tenable in this piece. A low value of ϵ_B ($\sim 10^{-4} - 10^{-3}$) indicates a weak magnetic field, especially for GRB 090902B and GRB 080916C. These GRBs have been studied by Kumar & Barniol Duran (2009), whose inferred magnetic field (along with several other LAT-detected events) is consistent with shock compression of a modest circumstellar field ($B \gtrsim 30\mu$G). That is to say, no dynamo process is necessary to generate the magnetic field needed for the observed synchrotron afterglow emission. In our best fittings, we find $B > 184\mu$G for GRB090902B and $B > 140\mu$G for GRB080916C even when $T_0 + 10^7$s, being broadly consistent with the results of Piran & Nakar (2010) and Li (2010). Meanwhile, when the blast wave enters the constant-density circumburst medium, the preshock magnetic field can be calculated with our fitting parameters as $B = (2\pi m_p \epsilon_B n)^{1/2} \approx 5\mu$G for 090902B and 4μG for 080916C, that suggests no magnetic field amplification.

(3) Although the ratio of ϵ_e and ϵ_B is large, synchrotron self-Compton is not significantly contributed to the observed flux density in the GeV band because of the Klein-Nishina suppression effect. In our sample fittings, ν_{KN} is less than $\nu_{IC,c}$ and $\nu_{IC,\min}$ until several hours later (when the flux is below the sensitivity of LAT). Hence, only synchrotron radiation from the external forward shock is enough to contribute to the high energy emission and the synchrotron self-Compton component can be neglected because $Y \ll 1$ in this piece. In particular, for GRB 090902B, from our best-fitting parameters, the maximum electron Lorentz factor at 82s indicates the highest photon energy can be as high as ~ 35 GeV, so it is plausible that 33 GeV photon may result from synchrotron radiation.

(4) The wind parameter for three longest bursts is $A_{35.5} \sim 10^{-2} - 10^{-1}$, which is reliably low. According to Dai & Wu (2003), the progenitor star of GRB 080916C, GRB 090902B, and GRB 090926A could have been in a cloud. Due to a high pressure of the cloud, a speedy wind will be slowed down by a pair of shocks (viz, a reverse shock that propagates into the wind gas and a forward shock that propagates into the cloud). This interaction produces a stellar wind bubble and forms a density-jump at a radius of $\sim 10^{18}$ cm. The homogeneous density outside this jump is estimated to be in the range of $n \sim 10^{-2} - 10^{-5}$, which is much less than the observed value of medium, but could not be excluded from the possibility of existence in areas of active star formation as the interiors of a prexisting superbubble (Panaitescu & Kumar 2001; Scalo & Wheeler 2001). If confirmed by the superbubble observation, this can provide a piece of evidence for a connection between long-duration GRBs and broad-lined SNe Ib/c. and would be natural to expect that massive progenitors of GRBs explode where we observe star formation. Meanwhile, in other fitting works (Cenko et al. 2010; Liu & Wang 2010), they have also confronted with the problem of low density, and suggest the lower metallicity progenitors with minimal pre-explosion mass loss or selection effects (Cenko et al. 2010). Hence, although the LAT emission at least during T_{90}, from the spectral perspective (Zhang et al. 2010), is likely to connect to the GBM emission of internal origin, the fitting facts tentatively suggest a possibility that the LAT observation records an internal-external shock transition and at least in the LAT decaying phase the external forward shock emission is dominated.

5. Conclusions and discussions

It is widely believed that long duration gamma-ray bursts (GRBs), like hydrogen-deficient Type Ib/c supernovae (SN Ib/c), result from the core collapse of a massive star. The main characteristic of setting GRBs apart from other SNe is that a substantial fraction of the explosive energy is coupled to relativistic ejecta. A compact central engine is

responsible for accelerating and collimating a jet-like outflow and driving a SN explosion (Woosley & Bloom 2006; Gehrels et al. 2009; Soderberg et al. 2010). The precise nature of the central engine which powers GRB-SNe, however, remains an open question.

In this paper, we have undertaken extensive broadband (>100 MeV, radio, optical, and X-ray) observations of three long-duration GRBs (GRB 080916C, GRB 090902B, GRB 090926A) detected by the LAT instrument on the Fermi satellite. A lower limit of the bulk Lorentz factor shown in Table 1 implies that the fireball is ultra-relativistic, which indicates that hyper-energetic bursts carry as high as $E_{iso} \sim 10^{55}$ ergs in the blast wave. The temporal indices α and spectral indices β in Table 2, which are consistent with the observed simple power law slope, show that our detailed density transition consideration can reconcile the plateau and shallower decay in the later afterglow. Table 3 displays the estimated physical parameter space of the best fit, which is all reasonably certificated by the theory mentioned in §4. Specifically, the wind parameter $A_{35.5} \sim 10^{-2} - 10^{-1}$ shed us light on the central engine of stellar collapsars and their association with SNe Ib/c (MacFadyen & Woosley 1999;Woosley & Heger 2006;Modjaz et al. 2008).

Furthermore,the tricky yet popular early rise of the LAT (>100MeV) light curve may indicate whether high energy photons share the same source as the low energy afterglows. Aside from two main kinds of explanation we mentioned above, leptonic or baryonic models, an alternative possibility comes from the high-latitude prompt emission (Kumar & Panaitescu 2000) and thus the flux density evolves as $F_\nu(t) \propto t^{-2-\beta}$. However, according to $\beta_{ob,LAT}$ in Table 2, the calculated temporal index is too steep to explain the early high energy emission decay. If the GeV component results from the same conventional unstructured ejecta as the late X-ray and optical afterglows, before the deceleration time ($t < t_{dec}$, that is, we only consider the thin shell case for long bursts), in the early wind bubble $n \propto R^{-2}$, the bulk Lorentz factor is nearly constant, and thus the electronic cooling and minimum frequencies evolve as $\nu_c \propto t$ and $\nu_{\rm min} \propto t^{-1}$, the peak flux density $F_{\rm max} \propto t$. Even when the SSC makes a significant effect, the IC electronic cooling and minimum frequencies and IC peak flux density $\nu_{IC,c} \propto t^3$ and $\nu_{IC,\rm min} \propto t^{-1}$ and $F_{IC,\rm max} \propto t^{-1}$. Since $\nu_{IC,c} > \nu_{IC,m} > \nu_{LAT} > \nu_c > \nu_m$ around the peak of LAT light curve, $F_{syn} \propto t^{1-p/2}$ (for $p > 2$) and $F_{IC} \propto t^{1/3}$. This is inconsistent with the observed rise of the LAT light curve, letting alone take the KN cutoff into account. Consequently, the unstructured ejecta can be excluded by the observed early rise.

Our explanation for the initial rising part is simply based on the assumption that $\Gamma \propto t^s$. Therefore, $\nu_c \propto t^{s+1}$, $\nu_m \propto t^{s-1}$, and $F_{syn} \propto \frac{1-e^{-\tau_{\gamma\gamma}}}{\tau_{\gamma\gamma}} t^{(sp-p+4s+2)/2}$ when $\nu_{GeV} > \nu_m > \nu_c$, while $F_{syn} \propto \frac{1-e^{-\tau_{\gamma\gamma}}}{\tau_{\gamma\gamma}} t^{(2-p)/2}$ when $\nu_{GeV} > \nu_c > \nu_m$. This assumption can be understandable within the framework of of the core collapse of a massive star (i.e., SNe Ib/c). If the central engine

ejects matter continuously, a clean tunnel would be leaving after the early ejecta sweeps up the stellar envelope, and the succeeding ejecta, whose energy is attained via continuous accretion even after the LAT trigger and whose Lorentz factor is larger, catches up with the early ejecta and injects more energy into the blast wave, giving rise to a rise of the LAT light curve.

In particular, as to GRB090902B, one of the tricky properties is its soft-hard-soft quasi-thermal spectrum evolution, since the soft-hard evolution appears within T_{90}, it can be better understood by our model that the initial outflow was dissipated as thermal component by the denser shock front/photosphere, when it breaks out of the envelope, the consequent highly relativistic ejecta in a clean tunnel can be dissipated strong enough to produce energetic non-thermal emission, even the photosphere can be outshined to some extent, therefore, the spectrum evolves from soft to hard.

Acknowledgements

This work is supported by the National Natural Science Foundation of China (grants 10873009 and 11033002) and the National Basic Research Program of China (973 program) No. 2007CB815404.

REFERENCES

Abdo, A. A., et al. 2009, Science, 323, 1688

Abdo, A. A., et al. 2009, ApJ, 706, L138

Asano, K., Guiriec, S.,& Mészáros, P. 2009, ApJ, 705, L191

Atwood, W. B., et al. 2009, ApJ, 697, 1071

Band, D., et al. 1992,Experimental Astronomy, 2, 307

Bissaldi, E., & Connaughton, V. 2009, GRB Coordinates Network, 9866, 1

Cenko, S. B., et al. 2010, arXiv:1004.2900

Chakrabarti, S. K., et al. 2009, GRB Coordinates Network, 10009, 1

Chandra, P., & Frail, D.A. 2009, GRB Coordinates Network, 9889, 1

Chevalier, R. A., & Li, Z.-Y. 2000, ApJ, 536, 195

Dai, Z. G., & Lu, T. 1998a, A&A, 333, L87-L90

Dai, Z. G., & Lu, T. 1998b, MNRAS, 298, 87

Dai, Z. G., & Lu, T. 2002, ApJ, 565, L87

Dai, Z. G., & Wu, X. F. 2003, ApJ, 591, L21

Evans, P. A., et al. 2007, A&A, 469, 379

Evans, P. A., et al. 2009, MNRAS, 397, 1177

Evans, P. A., et al. 2009, GRB Coordinates Network, 9871, 1

Fenimore, E. E., Madras, C. D., & Nayakshin, S. 1996, ApJ, 473, 998

Gao, W.-H., Mao, J., Xu, D., & Fan, Y.-Z. 2009, ApJ, 706, L33

Gehrels, N., et al. 2004, ApJ, 611, 1005

Gehrels, N., Ramirez-Ruiz, E., & Fox, D. B. 2009, ARA&A, 47, 567

Golenetskii, S., et al. 2009a, GRB Coordinates Network, 9049, 1

Granot, J., for the Fermi LAT Collaboration, & the GBM Collaboration 2010, arXiv:1003.2452

Greiner, J., et al. 2009, A&A, 498, 89

Gupta, N., & Zhang, B. 2007, MNRAS, 380,78

Jin, Z. P., Xu, D., Covino,S., D'Avanzo, P., Antonelli, A., Fan, Y. Z., & Wei, D. M. 2009, MNRAS, 400, 1829

Kennea, J. A., & Stratta, G. 2009, GRB Coordinates Network, 9868, 1

Kumar, P., & Barniol Duran, R. 2009, MNRAS, 400, L75

Kumar, P., & Barniol Duran, R. 2010, MNRAS, 1243

Kumar, P., & Panaitescu, A. 2000, ApJ, 541, L51

Lazzati, D., Rossi, E., Covino, S., Ghisellini, G., & Malesani, D. 2002, A&A, 396, L5

Li, Z. 2010, eprint arXiv, 1004, 791, 6 pages

Liu, R.Y., & Wang, X.Y. 2010, ApJ, submitted (arXiv:1009.1289)

MacFadyen, A. I., & Woosley, S. E. 1999, ApJ, 524, 262

MacFadyen, A. I., Woosley, S. E., & Heger, A. 2001, ApJ, 550, 410

Mészáros, P., & Rees, M. J. 1997, ApJ, 476, 232

Meegan, C., et al. 2009, ApJ, 702, 791

Modjaz, M., et al. 2008, AJ, 135, 1136

Noda, K., et al. 2009, GRB Coordinates Network, 9951, 1

Panaitescu, A., & Kumar, P. 2001, ApJ, 554,667

Panaitescu, A., & Kumar, P. 2002, ApJ, 571, 779

Pandey, S. B., et al. 2010, ApJ, 714, 799

Perri, M., Preger, B., & Stratta, G. 2008, GRB Coordinates Network, 8261, 1

Piran, T., & Nakar, E. 2010, ApJ, 718, L63

Rau, A., et al. 2010,ApJ, submitted (arXiv:1004.3261)

Razzaque, S., Dermer, C. D., & Finke, J. D. 2009, arXiv:0908.0513

Rees, M. J., & Meszaros, P. 1998,ApJ, 496, L1

Ryde, F., et al. 2010, ApJ, 709, L172

Sari, R., Piran, T., & Narayan, R. 1998, ApJ, 497, L17

Sari, R., & Esin, A. A. 2001, ApJ, 548, 787

Scalo, J., & Wheeler, J. C., 2001, ApJ, 562, 664

Soderberg, A. M., et al. 2010, Nature, 463, 513

Spergel, D. N., et al. 2007, ApJS, 170, 377

Stratta, G., D'Elia, V., & Perri, M. 2009, GRB Coordinates Network, 9876, 1

Swenson, C. A., et al.& Siegel, M. H. 2009, GRB Coordinates Network, 9877, 1

Swenson, C. A., et al. 2010, ApJ, 718, L14

Tam, P. H., Pun, C. S. J., Huang, Y. F., & Cheng, K. S. 2005, New A, 10, 535

Terada, Y.,et al. 2009, GRB Coordinates Network, 9897, 1

Toma, K., Wu, X.-F., & Mészáros, P. 2009, ApJ, 707, 1404

Uehara, T.,Takahashi,H., & McEnery, J. 2009, GRB Coordinates Network, 9934, 1

van der Horst, A. J., Kamble, A. P., Wijers, R. A. M. J., & Kouveliotou, C. 2009, GRB Coordinates Network, 9883, 1

Vetere, L. 2009, GRB Coordinates Network, 9961, 1

Wang, X. Y., Li,Z., Dai, Z. G.,& Meszaros, P. 2009, ApJ, 698, 198

Wang, X. Y., He,H N., Li,Z.,& Dai, Z. G. 2010, ApJ, 712, 1232

Woosley, S. E., & Bloom, J. S. 2006, ARA&A, 44, 507

Woosley, S. E., & Heger, A. 2006, ApJ, 637, 914 5

Wu, X. F., Dai, Z. G.,Huang, Y. F., & Lu, T. 2005, ApJ, 619, 968 5

Zhang, B., & Pe'er, A. 2009, ApJ, 700,L65

Zhang, B.-B., et al. 2010, ApJ, submitted (arXiv: 1009.3338)

Zou, Y.-C., Fan, Y.-Z.,& Piran, T. 2009, MNRAS, 396, 1163

This preprint was prepared with the AAS LaTeX macros v5.2.

GRBs	z	E_p(MeV)	F_h(ergcm^{-2})	T_{90}(s)	$\alpha_{\rm band}$	$\beta_{\rm band}$	E_{max}(MeV)	t_{dec}(s)	$\eta(>)$
080916C	4.35	1.443	1.55×10^{-4}	100	-1.027	-2.36	13.2×10^3	5	460
090902B	1.82	0.7	3.10×10^{-4}	53	-0.83	-3.68	11.2×10^3	7	450
090926A	2.11	0.412	1.93×10^{-4}	100	-0.749	-2.442	19.6×10^3	16	320

Table 1: Lower limit of the Lorentz factor at deceleration time, the redshift z, the peak energy of Band function E_p Band function indices $\alpha_{\rm band}$ and $\beta_{\rm band}$ and the maximum energy of photons in the prompt emission phase E_{peak} are from Zhang et al. (2010)

GRBs	α_{LAT}	$\alpha_{ob,LAT}$	β_{LAT}	$\beta_{ob,LAT}$	$\alpha_{x,o,1}$	$\alpha_{x,o,2}$	$\alpha_{ob,x}$	$\alpha_{ob,o}$	$\beta_{x,o}$	$\beta_{ob,x}$	$\beta_{ob,o}$
$080916C^a$	1.48	1.33 ± 0.08	1.16	1.1 ± 0.1	1.49	0.99	1.29 ± 0.09	1.40 ± 0.05	0.66	0.50 ± 0.16	0.38 ± 0.02
$090902B^b$	1.47	1.40 ± 0.06	1.16	$-\clubsuit$	1.49	0.98	1.36 ± 0.03	0.89 ± 0.05	0.65	0.90 ± 0.13	0.76 ± 0.07
$090926A^c$	2.01	2.05 ± 0.14	1.5	$1.26^{+0.22}_{-0.24}$	2.00	1.50	$^\star 1.43 \pm 0.03$	$^\star 1.38 \pm 0.02$	1.00	$1.12^{+0.2}_{-0.13}$	1.03 ± 0.05

Table 2: According to $F_\nu \propto t^{-\alpha}\nu^{-\beta}$

, α_{LAT}, $\alpha_{x,o,1}$, $\alpha_{x,o,2}$ are the estimated temporal indices of the LAT band photons, X-ray + optical photons in the wind bubble, and X-ray + optical photons in the homogeneous medium from our best-fit parameters. $\alpha_{ob,LAT}$, $\alpha_{ob,x}$, $\alpha_{ob,o}$ are the observed temporal indices of GeV photons, simple power-law X-ray photons and optical photons. β_{LAT} and $\beta_{x,o}$ are the estimated spectral indices of the LAT band photons and X-ray + optical photons in either medium from our best-fit parameters. $\beta_{ob,LAT}$, $\beta_{ob,x}$, and $\beta_{ob,o}$ are the observed spectral indices of GeV photons, simple power-law X-ray photons and optical photons. High energy data are taken from Zhang et al. (2010), X-ray data are taken from Swift Group (Evans et al. 2007; Evans et al. 2009). In addition, a is taken from Greiner et al. (2009), b is from Pandey et al. (2010), c is from Swenson et al. (2010), $-\clubsuit$ represents no data available.For 090926A, the temporal slope of the X-ray and optical band in Rau et al. (2010) is: $\alpha = 1.6 \pm 0.2$ before the first flare, $\alpha = 1.75 \pm 0.04$ after the second flare, and $\alpha = 1.63 \pm 0.01$ between, which is consistent with our estimated value.

GRBs	p	s	$E_{K,iso,55}$	η_3	$A_{\star,35.5}$	ϵ_e	ϵ_B	ξ	t_{break}(s)	t_{end}(s)	t_{jet}(s)	ς_γ	R_{break}(cm)	$n_{after}(cm^{-3})$
080916C	2.32	0.5	3.16	0.8	10^{-1}	0.3	1.3×10^{-6}	2.3	$10^{5.3}$	$10^{5.6}$	–	21.8%	7.36×10^{18}	1.27×10^{-3}
090902B	2.3	0.5	0.79	0.8	10^{-2}	0.2	1.0×10^{-4}	2.0	$10^{5.1}$	$10^{6.0}$	$10^{6.0}$	32.4%	1.64×10^{19}	2.21×10^{-5}
090926A	3.0	0.2	2.74	0.55	10^{-1}	0.35	4.5×10^{-6}	2.5	$10^{4.8}$	$10^{4.9}$	–	7.1%	7.37×10^{18}	1.38×10^{-3}

Table 3: The left part of the table are best-fit parameters for GRB080916C, GRB090902B, and GRB090926A, the right part are prompt emission energy fraction, radius when a density jump occurs and circumburst density after the jump, respectively.

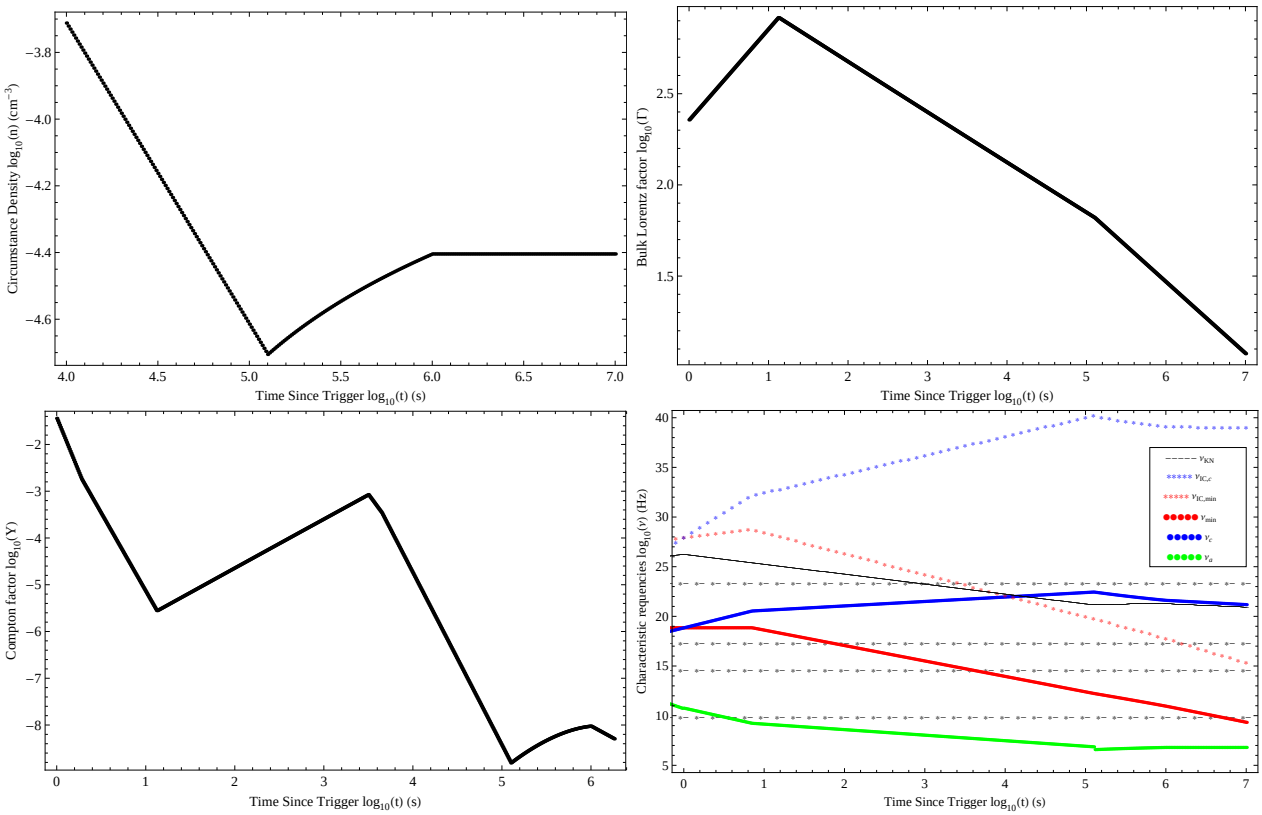

Fig. 1.— Physical parameter evolution with the best fit parameter for GRB090902B, similar to the other two bursts. Upper-left panel: a. circumburst density with radius, upper-right panel: b. blast wave bulk Lorentz factor with time; lower-left panel: c. Compton Y factor ($\ll$1 due to KN effects) with time; lower-right panel: d. characteristic frequency evolution.

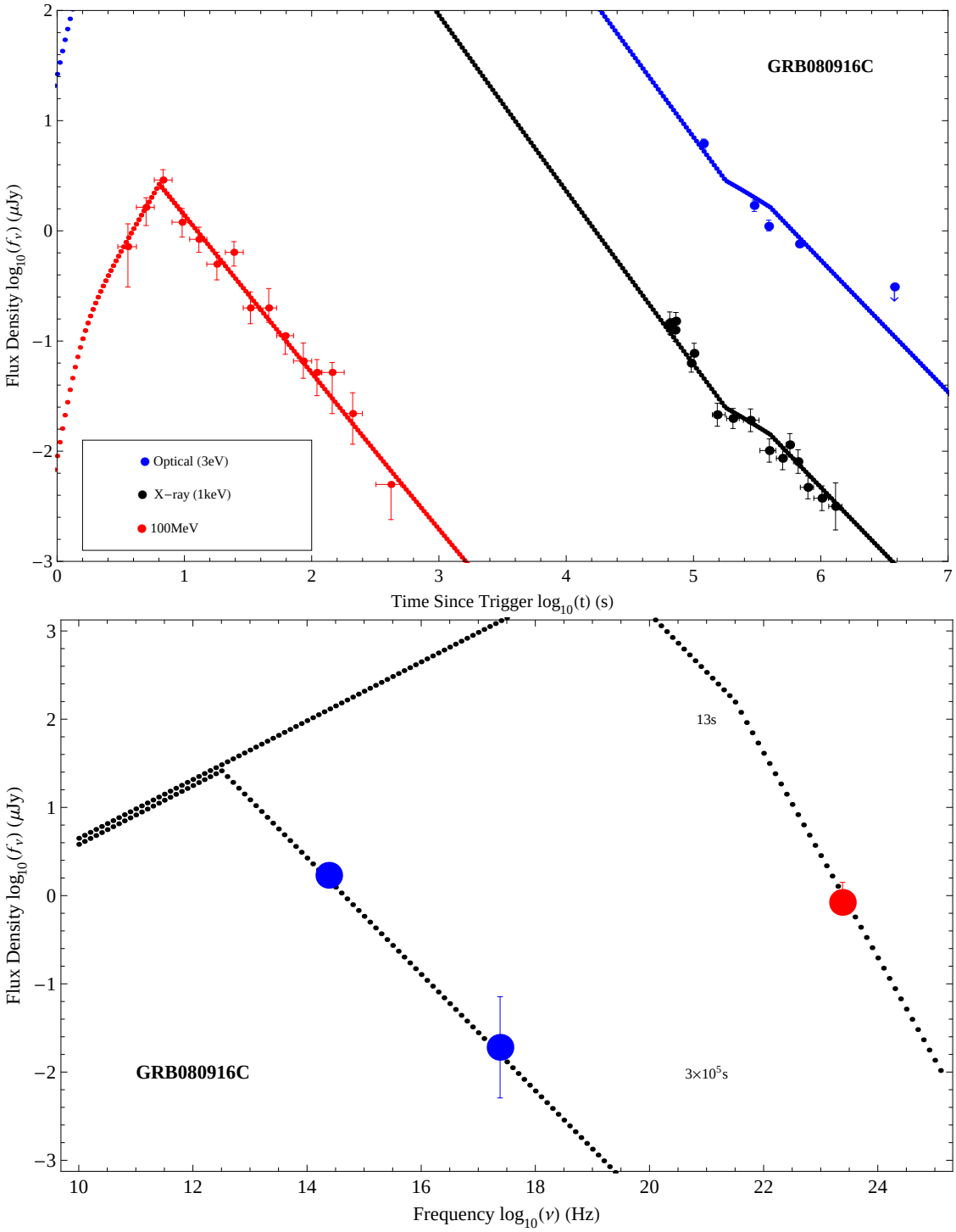

Fig. 2.— Best fit for GRB 080916C: $p = 2.32$, $s = 0.5$, $E^{iso}_{K,55} = 3.16$, $\eta_3 = 0.8$, $A_{35.5} = 10^{-1}$, $\epsilon_{e,0} = 0.3$, $\epsilon_{B,0} = 1.31 \times 10^{-6}$, $\varepsilon = 2.3$, $t_{break} = 10^{5.3}$ s, $t_{end} = 10^{5.6}$ s, no jet break appears during the modeling period

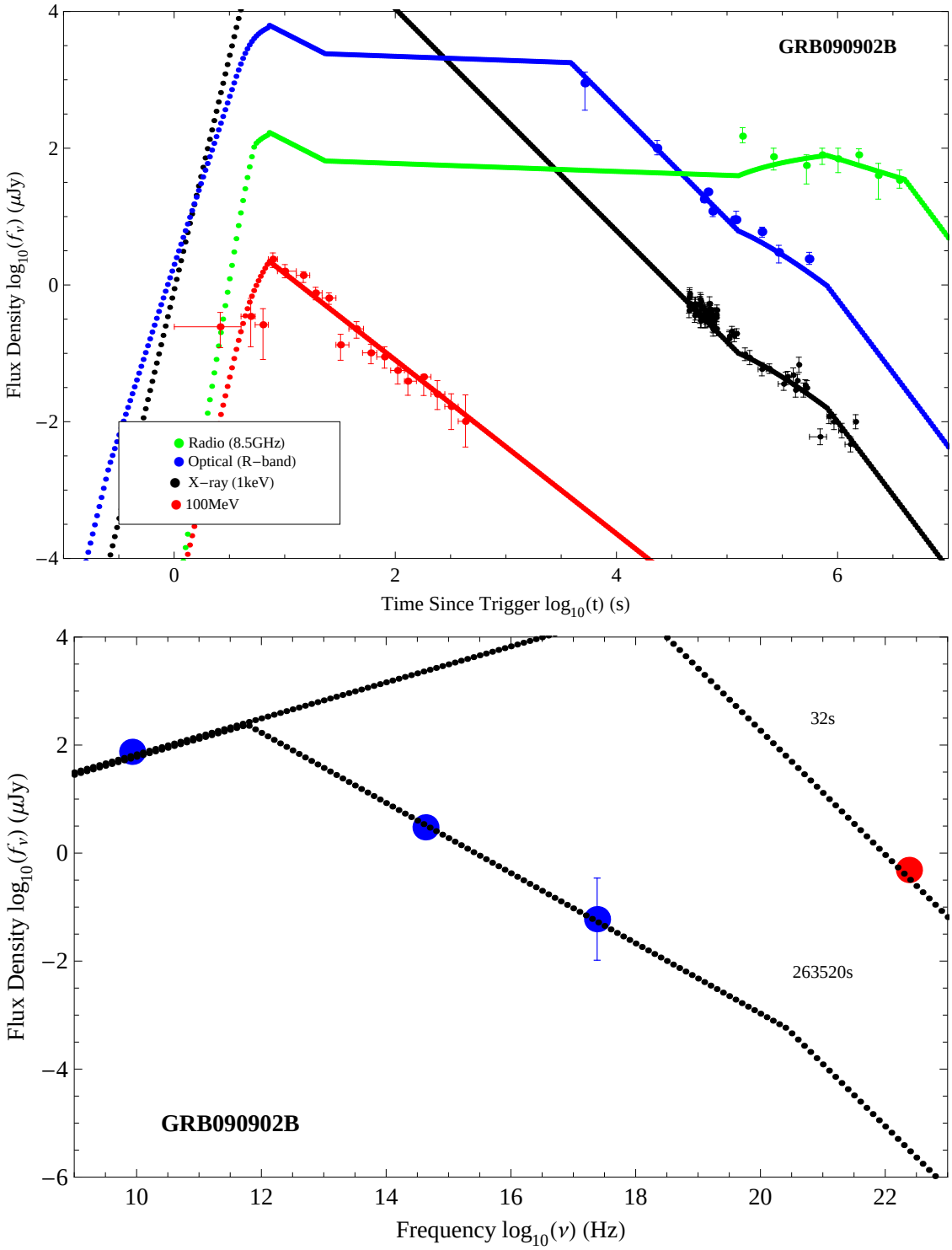

Fig. 3.— Best fit for GRB 090902B: $p = 2.3$, $s = 0.5$, $E^{iso}_{K,55} = 0.8$, $\eta_3 = 0.8$, $A_{35.5} = 10^{-2}$, $\epsilon_{e,0} = 0.2$, $\epsilon_{B,0} = 10^{-4}$, $\varepsilon = 2.0$, $t_{break} = 10^{5.1}$ s, $t_{end} = 10^{6.0}$ s, $t_{jet} = 10^{6.0}$ s

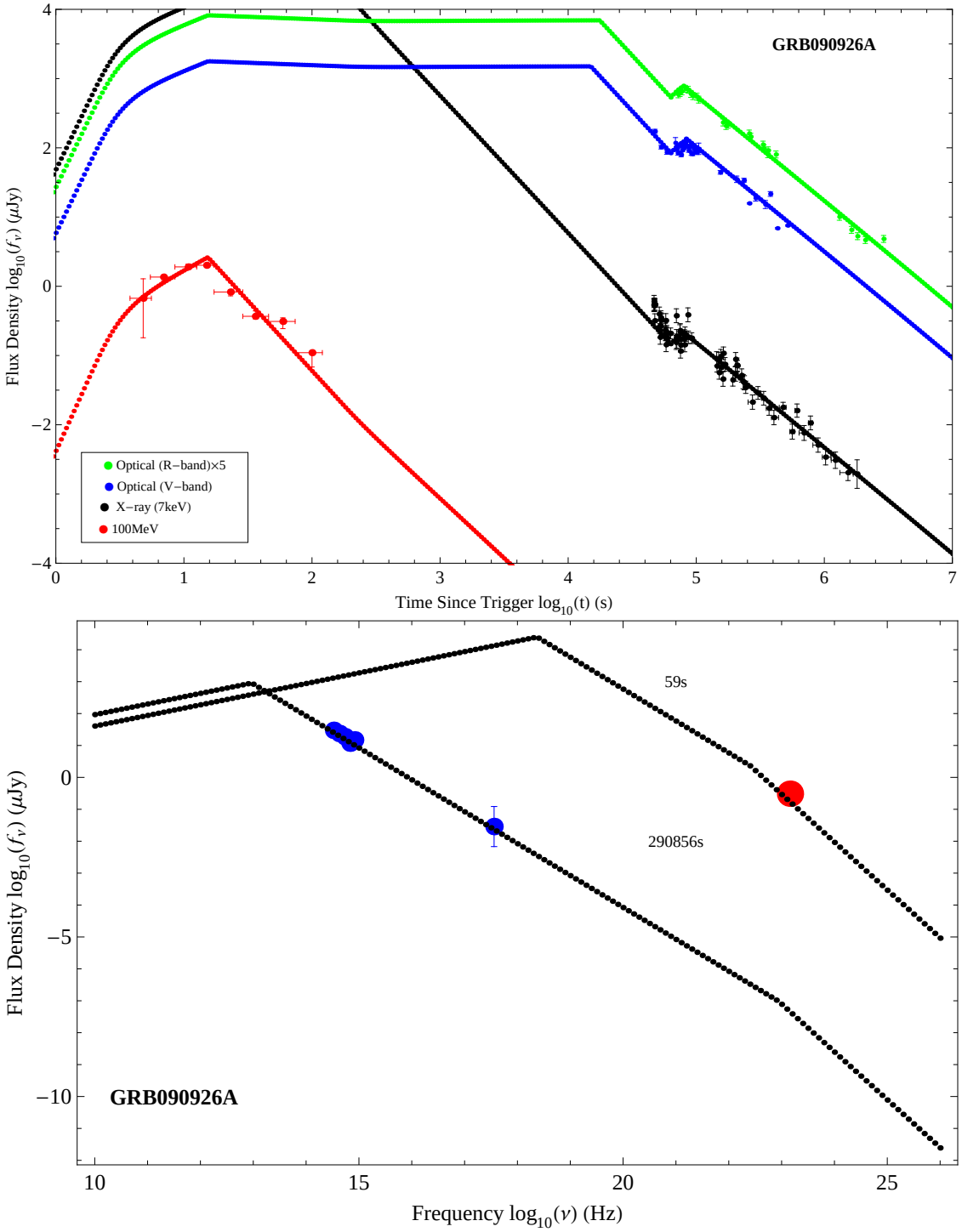

Fig. 4.— Best fit for GRB 090926A: $p = 3.0$, $s = 0.2$, $E^{iso}_{K,55} = 2.74$, $\eta_3 = 0.55$, $A_{35.5} = 10^{-1}$, $\epsilon_{e,0} = 0.35$, $\epsilon_{B,0} = 4.5 \times 10^{-6}$, $\varepsilon = 2.5$, $t_{break} = 10^{4.8}$ s, $t_{end} = 10^{4.9}$ s, no jet break confirmed until 21 days